Data-dependent absorbing boundaries

John Toldi and Dave Hale

Abstract

We derive a data-dependent difference equation for use at the edges of the computational grid in finite-difference migration or modelling programs. We demonstrate the ability of this equation to attenuate unwanted boundary reflections with several examples.

Introduction

Due to the finite grid size required for any computer implementation of a finite difference migration or modelling scheme, some consideration must be given to the choice of side boundary conditions. The simplest boundary conditions are obtained by requiring the wavefield or its lateral first derivative to vanish at the boundary. Unfortunately, these so-called zero-value or zero-slope conditions reflect perfectly waves incident on the boundaries. So, Clayton and Enquist (1980) derived "absorbing" boundary conditions which attenuate boundary reflections. They use a boundary difference equation having a dispersion relation approximating that of the interior equation, the approximation being best for outgoing waves. The desired result is that outgoing waves continue as if they had not encountered a boundary.

Before leaving Stanford and the SEP, Rob Clayton suggested another boundary equation that sounded promising. Unlike those published previously, this boundary equation would be data-dependent. In this paper, we derive this data-dependent absorbing boundary and illustrate its effectiveness with both synthetic and recorded wavefields.

Data-independent boundary conditions

In the notation of Clayton and Enquist (1980), their boundary equations are summarized by the following dispersion relations:

$$B1: \quad \frac{vk_x}{\omega} = b \tag{1}$$

$$B2: \quad \frac{vk_z}{\omega} = a - b\frac{vk_x}{\omega} \tag{2}$$

$$B3: \quad \frac{vk_z}{\omega} = \frac{a - b\dfrac{vk_x}{\omega}}{1 - \dfrac{cvk_x}{\omega}} \tag{3}$$

where a, b, and c are non-negative constants, v is velocity, ω is frequency, and k_x and k_z are horizontal and vertical wavenumbers, respectively. We leave the detailed explanation of these equations to the aforementioned paper, but note that they are designed to absorb downgoing waves incident on the right boundary (where z increases downward and x increases to the right). For upgoing waves, replace k_z with $-k_z$; for the left boundary, replace k_x with $-k_x$.

Equation (1) with $b = \sin\vartheta$ absorbs perfectly a plane-wave propagating at angle ϑ measured from the vertical. Setting $b = 0$ yields the zero-slope condition. A (z,x,ω)-domain implementation of equation (1) is

$$0 = q(z,n,\omega) - e^{\frac{i\omega b}{v}} q(z,n-1,\omega) \tag{4}$$

where $q(z,x,\omega)$ is the sampled wavefield, and $x = n$ defines the right boundary. (We assume unit sampling intervals.) As discussed by Thorson (1979), a z-independent boundary equation such as equation (4) may be incorporated into the adjacent interior equation via one step of Gaussian elimination. This procedure, which effectively moves the boundary off the computational grid, is commonly found in SEP programs (e.g., Kjartansson, 1978). For clarity in this paper, we chose not to use this trick but to include the boundary equation explicitly.

Figures 1a, 2a, and 3a demonstrate the annoying reflection of waves off the side boundaries when the zero-slope ($b = 0$) condition is used in a "45-degree", finite-difference wavefield extrapolation. Boundary reflections are attenuated considerably by using $b = \sin 30^\circ$ in equation (4), as illustrated in Figures 1b, 2b, and 3b. As expected, the 30-degree plane-wave of Figure 1b is absorbed perfectly.

Compared with equations (1) or (2), equation (3) better approximates (for outgoing waves) the semi-circular dispersion relation associated with the interior difference equation and, therefore, is capable of absorbing waves with a wider range of propagation angles. A finite-difference approximation to equation (3) yields the results shown in Figures 1c, 2c, and 3c. The constants in equation (3) were chosen to match the interior dispersion relation at angles of 0, 30, and 60 degrees. Reflections at all angles are virtually eliminated. An annoying feature of equation (3), however, is the way it handles waves propagating toward the interior, e.g., the unrealistic (unstable?) buildup of energy at the left boundary in Figures 1c and 2c.

Data-dependent boundary conditions

How should one choose the constants in equations (1), (2) and (3)? For the B3 condition, fitting equation (3) at 0, 30 and 60 degrees is reasonable since, as our synthetic results indicate, the resulting approximation is adequate at intermediate angles. For equations (1) or (4), however, the choice of the constant b is more critical. Clayton's parting suggestion was to interpret equation (4) as "predicting" $q(z,n,\omega)$ from $q(z,n-1,\omega)$. The "prediction coefficient" may be determined from data near the boundary by minimizing (in the manner of John Burg) $E(a)$ defined by

$$E(a) \equiv |q_{n-1} - a q_{n-2}|^2 + |q_{n-2} - a^* q_{n-1}|^2$$

(where, to simplify notation, we have omitted irrelevant z and ω subscripts). The minimizing a is

$$a = \frac{2 q_{n-1} q^*_{n-2}}{|q_{n-1}|^2 + |q_{n-2}|^2} \tag{5a}$$

The difference equation at the right boundary is then

$$0 = q_n - a q_{n-1} \tag{5b}$$

To see how this data-dependent prediction works, suppose the data consists only of a single plane-wave propagating at angle ϑ:

$$q(z,x,\omega) = q e^{i\omega\left[\frac{z\cos\vartheta}{v} + \frac{x\sin\vartheta}{v} - t\right]}$$

Equations (5) then yield the boundary equation

$$0 = q_n - e^{\frac{i\omega\sin\vartheta}{v}} q_{n-1}$$

which is just equation (4) "tuned" automatically to the correct propagation angle. Figures 1d, 2d, and 3d demonstrate the effectiveness of this data-dependent absorbing boundary condition for a variety of synthetic wavefields. By computing a new prediction coefficient a for each depth z, equations (5) absorb perfectly even the spherical wavefronts in Figure 3d. When equation (5a) predicts a wave propagating away from the boundary (e.g., at the left boundary in Figures 1 and 2), we reset a to correspond to the B1 condition of equation (4), set to absorb outgoing 30-degree plane-waves. Therefore, at the left boundary, Figures 2b and 2d are virtually identical.

The synthetic examples above demonstrate that data-dependent boundary equations perform well when only one propagation angle is present at a boundary at any given depth z. Recorded seismic wavefields, however, typically represent a superposition of plane-waves having many different propagation angles. To compare the performance of various boundary equations in a more realistic setting, we migrated the CMP-stacked section plotted in Figure 4 using zero-slope, B1, B3, and data-dependent boundary equations in a "45-degree", finite-difference migration program. The migrated sections are plotted in Figures 5a-d. As expected, any of the three absorbing boundaries tested performs better than the zero-slope condition (Figure 5a). Because the dip of the dominant reflectors in this section is about 22 degrees, the B1 condition set to 30 degrees (Figure 5b) performs quite well. The B3 condition (Figure 5c) nicely absorbs waves impinging on the boundaries, but leaves flat events with anomalously large amplitudes at the boundaries. Note that the data-dependent equations (Figure 5d) perform well, even in the presence of strong events dipping to the right and to the left at both boundaries.

Conclusion

By allowing the difference equation at finite-grid boundaries to be data-dependent, one enhances the ability of that equation to absorb incident waves.

REFERENCES

Clayton, R.W., and Enquist, B., 1980, Absorbing side boundary conditions for wave equation migration: Geophysics, v.45, p.895-904.

Kjartansson, E., 1978, Modeling and migration with the monochromatic wave equation -- variable velocity and attenuation: SEP-15, p.1-19.

Thorson, J., Stability of finite difference boundary conditions: SEP-20, p.165-178.

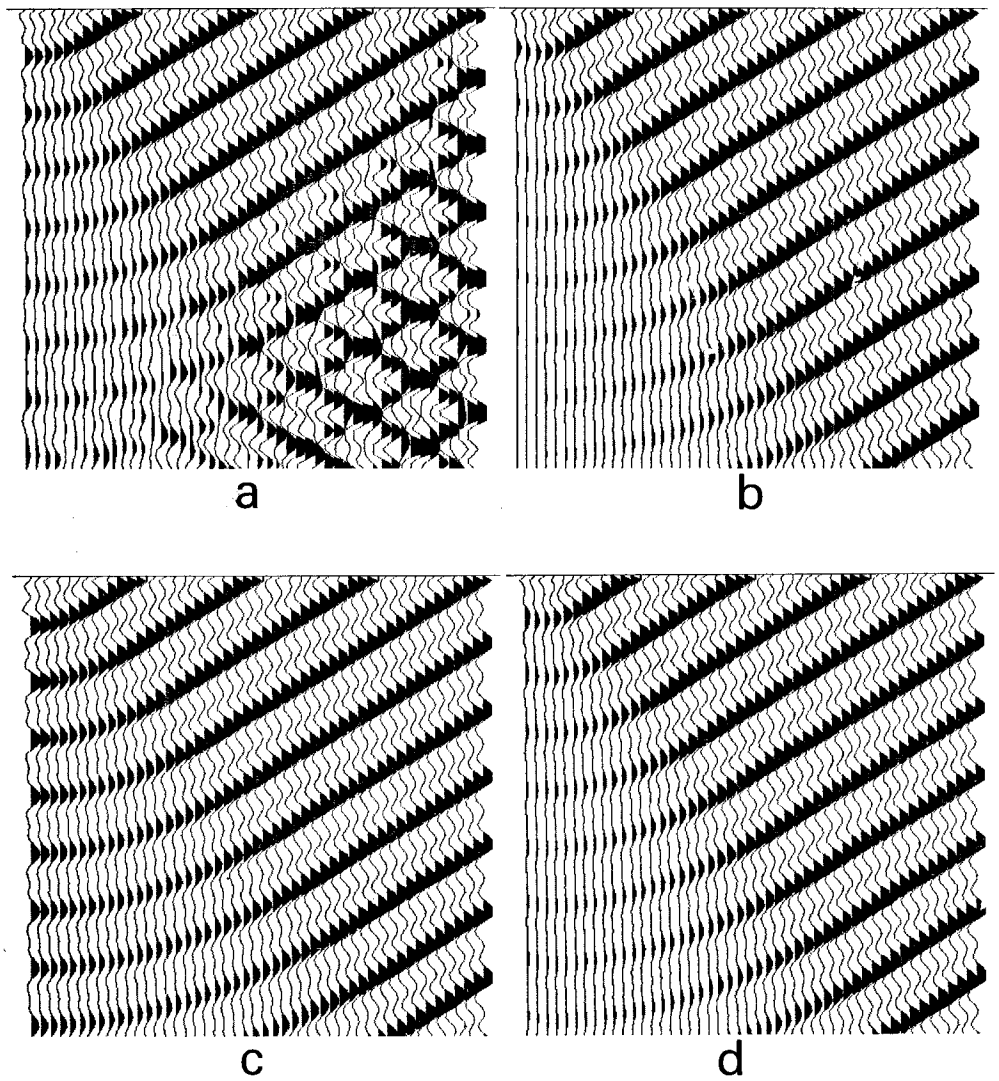

FIG. 1. Snapshots of 30-degree, downgoing plane-waves computed using (a) zero-slope, (b) B1, (c) B3, and (d) data-dependent boundary equations. Boundary reflections (a) are virtually eliminated by using any of the absorbing boundary equations. The B1 equation performs well (b) because it was set to perfectly absorb 30-degree plane waves. The B3 equation absorbs well (c) but poorly handles energy propagating away from the left boundary. The data-dependent equation also absorbs well (d); when incoming waves are detected by equation (5a), the data-dependent equation is reset to the 30-degree B1 equation.

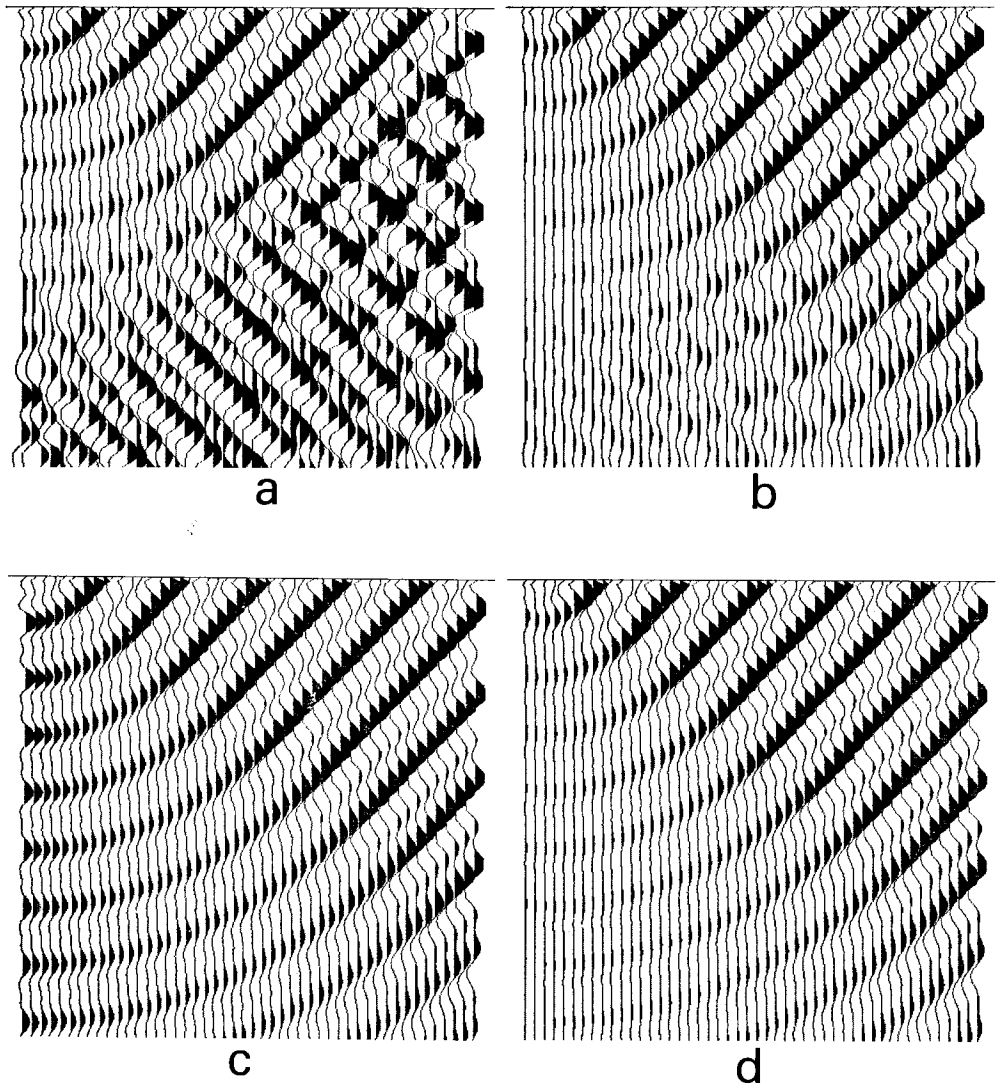

FIG. 2. Snapshots of 45-degree, downgoing plane-waves computed using (a) zero-slope, (b) B1, (c) B3, and (d) data-dependent boundary equations. The B1 equation, set to 30 degrees as in Figure 1b, slightly reflects the 45-degree wave (b). The data-dependent equation (d) is automatically tuned to the correct propagation angle and better handles energy at the left boundary than does the B3 condition (c).

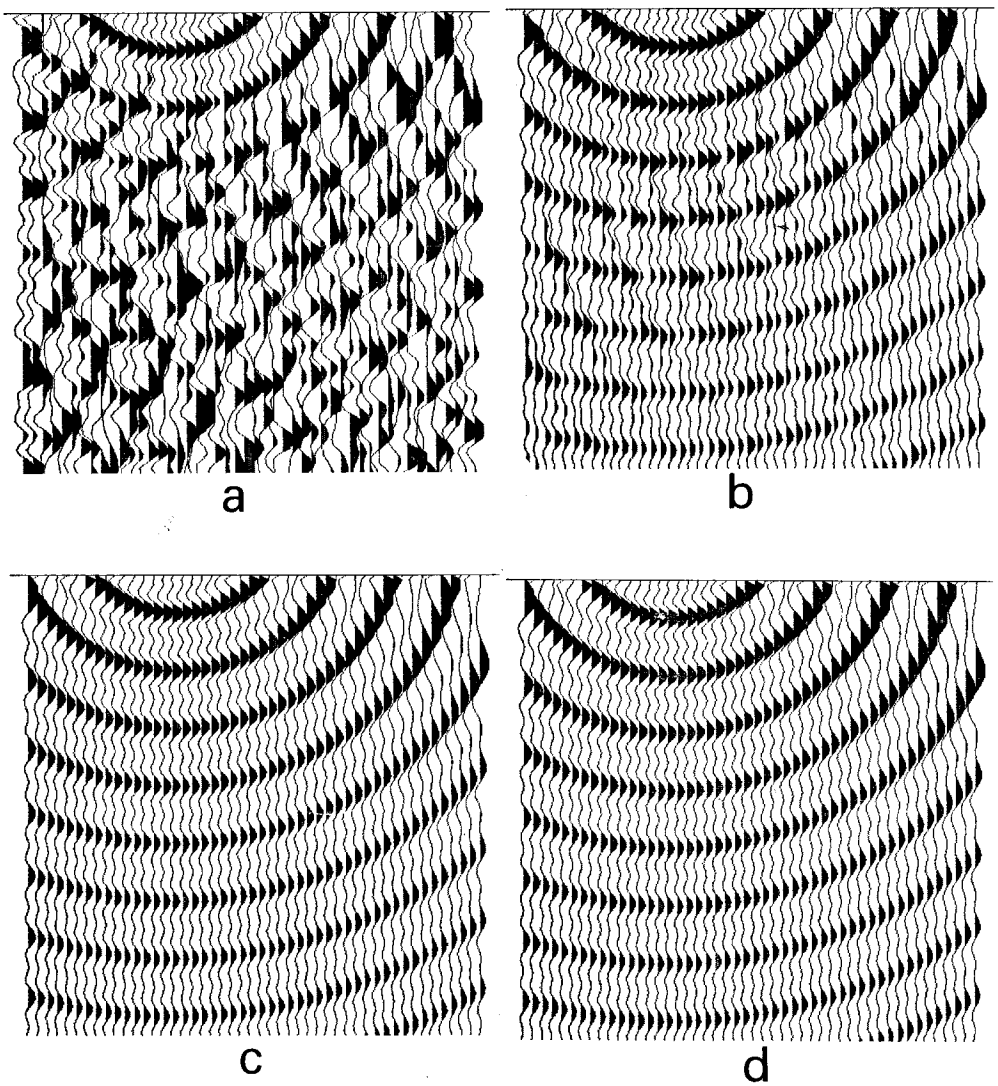

FIG. 3. Snapshots of expanding spherical waves computed using (a) zero-slope, (b) B1, (c) B3, and (d) data-dependent boundary equations. The B1 condition set to 30 degrees (b) cannot absorb the wide range of angles incident on the boundaries. Both the B3 (c) and data-dependent (d) conditions absorb well.

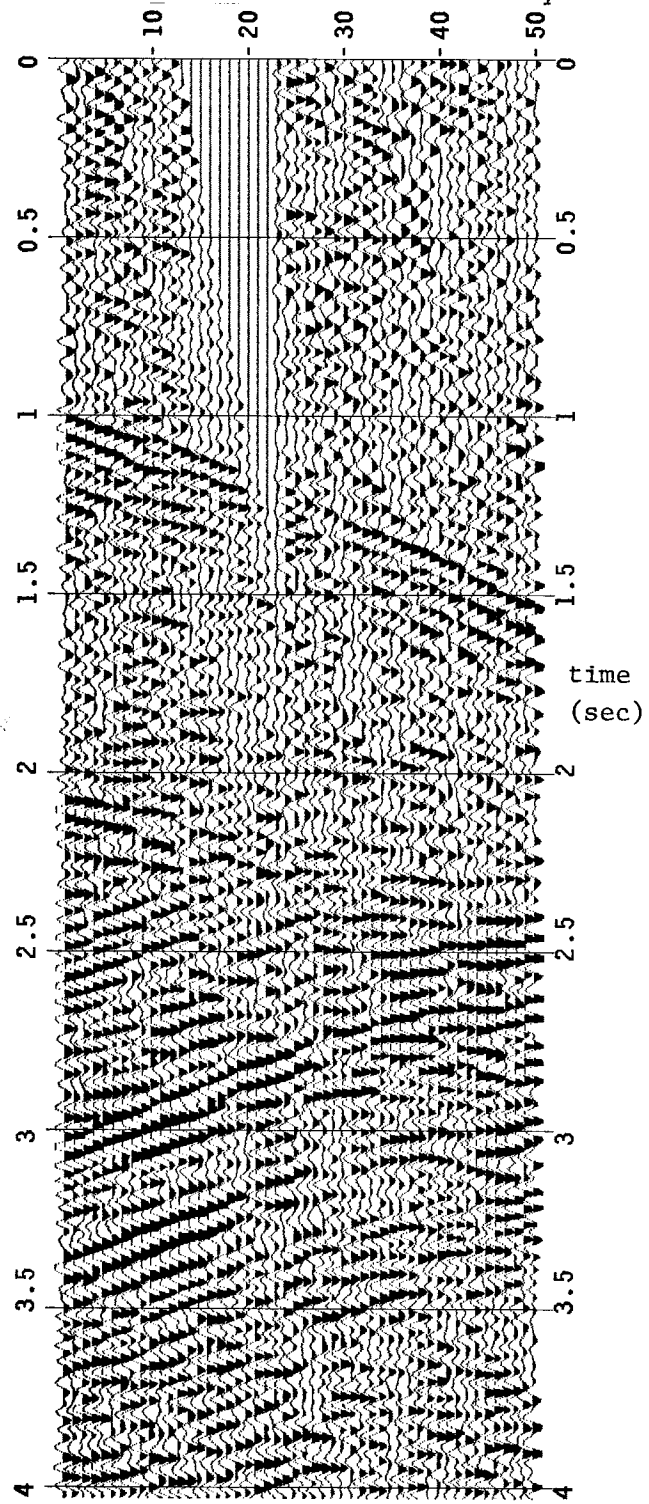

FIG. 4. A CMP-stacked section used to test several boundary conditions in finite-difference migration. Notice the strong events dipping both to the right and left. Most of this dipping energy should migrate off the section, provided the side boundaries are absorbing. This window of data was taken from a much longer section of the Wind River, Wyoming data recorded as part of the COCORP project.

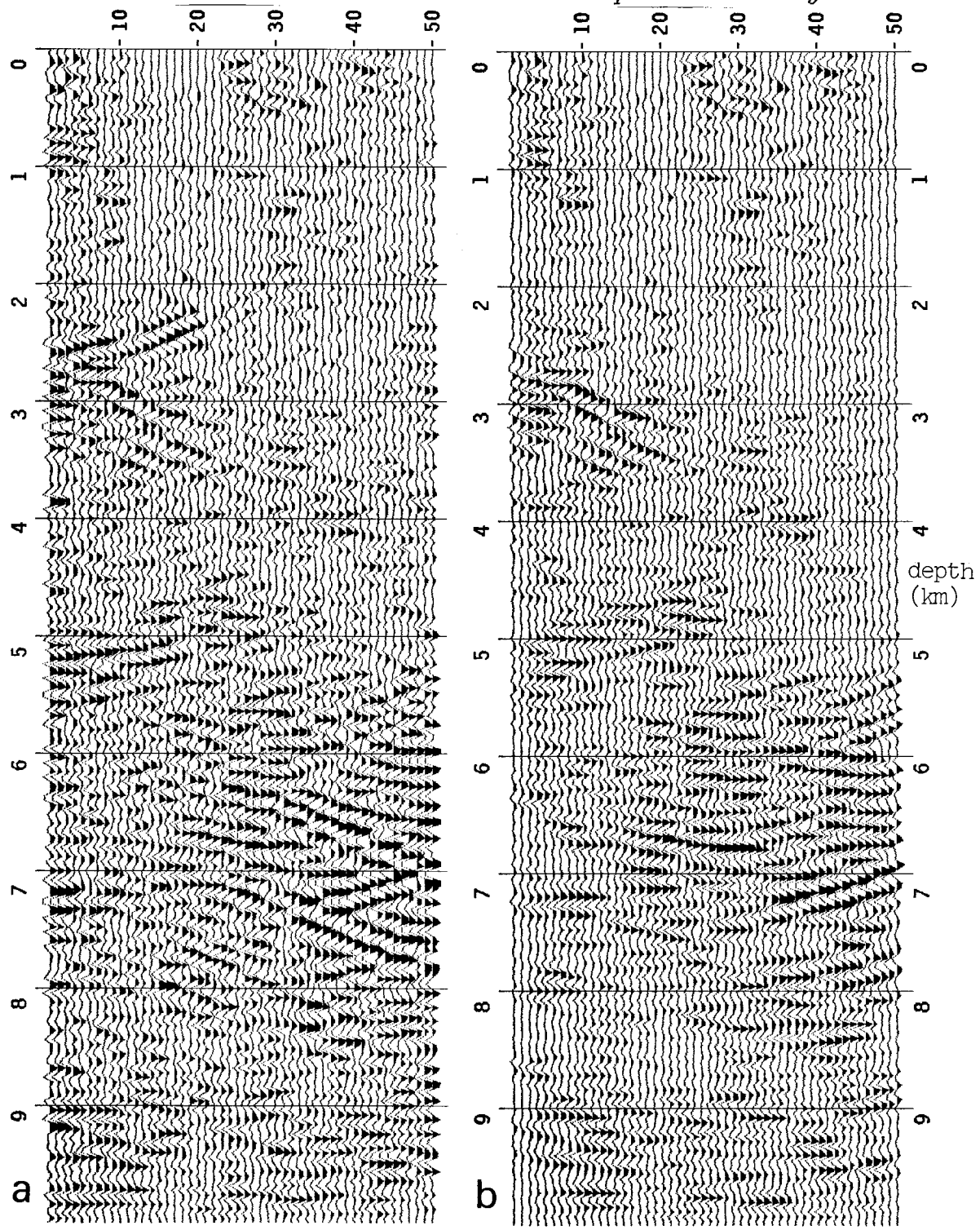

FIG. 5. The migrated sections computed using (a) zero-slope, (b) B1, (c) B3, and (d) data-dependent boundary conditions in a "45-degree", finite-difference migration program. Reflections off the boundaries (a) are significantly attenuated by any of the absorbing equations (b, c, or d). Note the anomalously strong flat events left at the boundaries by the B3 condition (c).

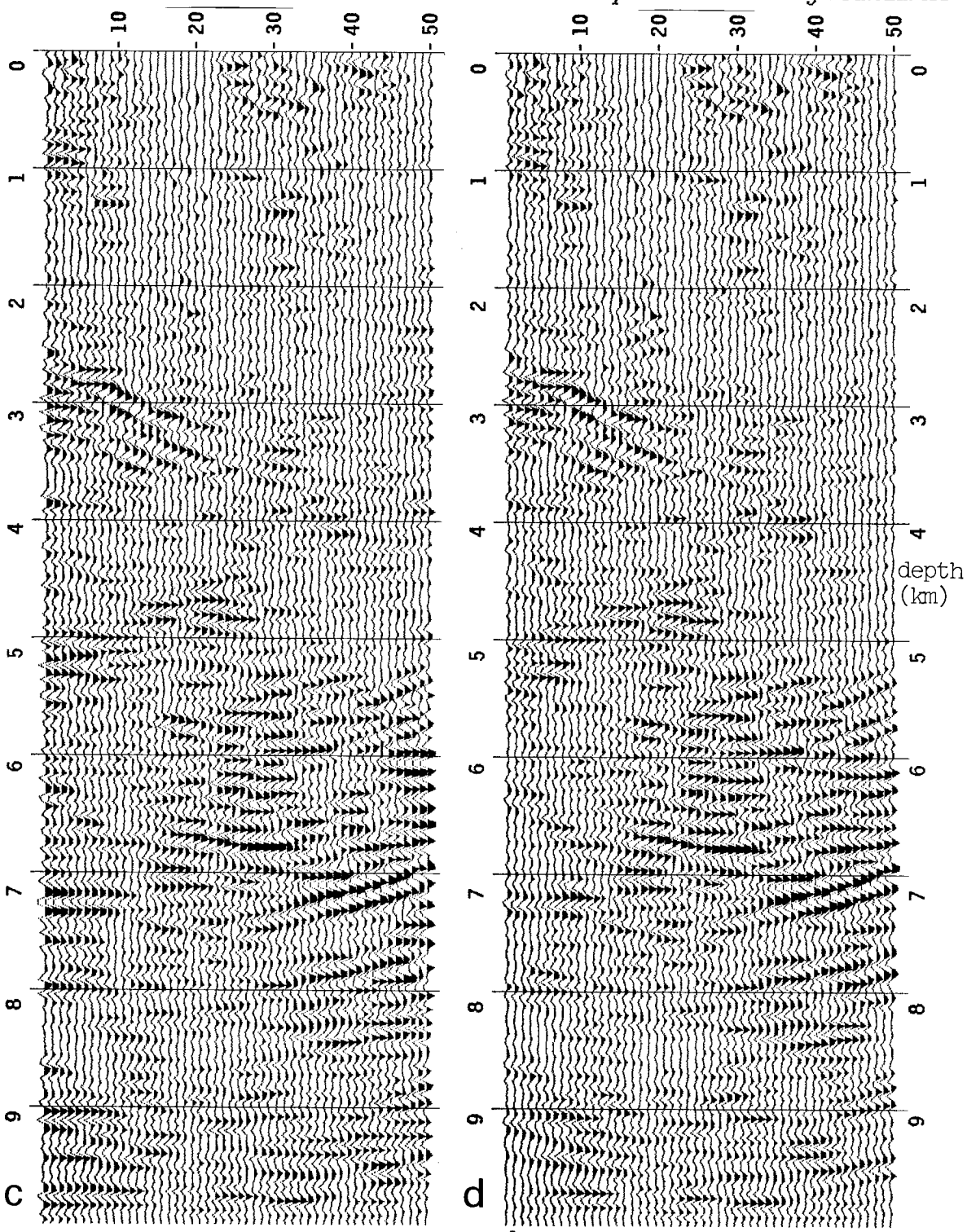
10
20
30
40
50
0
1
2
3
4
5
6
7
8
9
depth
(km)
c
d